Journal of Power Sources 208 (2012) 138–143

Contents lists available at SciVerse ScienceDirect

Journal of Power Sources

journal homepage: www.elsevier.com/locate/jpowsour

Electrochemical in situ polymerization of reduced graphene oxide/polypyrrole composite with high power density

Jingping Wang[a,b], Youlong Xu[a,*], Jianbo Zhu[a], Penggang Ren[c]

[a] Electronic Materials Research Laboratory, Key Laboratory of the Ministry of Education, Xi'an Jiaotong University, Xi'an 710049, China
[b] College of Chemistry and Chemical Engineering, Shaanxi University of Science and Technology, Xi'an 710021, China
[c] Institute of Printing and Packaging Engineering, Xi'an University of Technology, Xi'an, Shaanxi 710048, China

ARTICLE INFO

Article history:
Received 8 October 2011
Received in revised form 5 February 2012
Accepted 6 February 2012
Available online 13 February 2012

Keywords:
Graphene oxide
Polypyrrole
Composite
In situ polymerization
Supercapacitors

ABSTRACT

We demonstrate a novel method of in situ galvanostatic polymerization to prepare reduced graphene oxide (RGO)/polypyrrole composite (RGO–PPy) for supercapacitors electrode. The PPy and the RGO interact closely and form the composite with porous structure. The BET specific surface area of RGO–PPy reaches 108 $m^2 g^{-1}$. The RGO–PPy composites show the high protonation level on polypyrrole (PPy) ring (41.1%), which can be related to the doping of PPy by oxygen-containing groups in *RGO* sheet. The RGO–PPy electrodes exhibit good electrochemical performance. The specific capacitance of RGO–PPy electrodes still reaches 224 F g^{-1} at charge/discharge current density of 240 A g^{-1} within an electrochemical windows of 0.8 V in 3 M KCl aqueous solution. The specific power of RGO–PPy electrodes reaches 38.6 kW kg^{-1} when its specific energy reaches 2.5 Wh kg^{-1} in two-electrode cell. The RGO–PPy electrodes have good cycle stability and show less than 17% specific capacitance decay at a charge/discharge current of 30 A g^{-1} within an electrochemical windows of 0.8 V after 5000 cycles.

1. Introduction

Supercapacitors, also called ultracapacitors, provide a bridge between conventional capacitors with short charge-discharge times and batteries with longer discharge times [1,2]. Supercapacitors have high power density, long cyclic life, a wide thermal operating range and low maintenance cost, so they have several applications in portable electronic devices, medical devices and electronic vehicles [2,3]. Recently, many researches about supercapacitors have focused on the electrode material, including various forms of carbon, conducting polymers and transition metal oxides [4]. Among these materials, polypyrrole (PPy) has been considered a potential material for supercapacitors due to its high conductivity, long-term environmental stability, environmental friendliness, good electrochemical reversibility, low cost and facile synthesis [5,6]. However, the long-term cycle stability and charge/discharge rate of PPy needs to be improved further for the commercialization of PPy electrode [4,6,7].

Composites of PPy and several kinds of carbon nanomaterials, i.e. carbon fiber, carbon nanotubes and graphene, were usually prepared for improving its electrochemical performance [8–12]. Graphene, a unique two-dimensional carbon nanostructure, should be a very ideal backbone of composite due to its high electrical conductivity, high Young's modulus and a large theoretical specific surface area [13–16]. Moreover, graphene-based materials can be prepared by simple chemical processing of graphite [14,17]. Therefore, the preparation of graphene-based composites for supercapacitors has attracted great attention. Biswas et al. prepared multilayered nanoarchitecture of graphene nanosheets and PPy nanowires with a specific capacitance of 165 F g^{-1} at discharge current density of 1 A g^{-1} [11]. It is obvious that the specific capacitance of this composite should be improved further. Zhang et al. synthesized graphene and PPy composites using an in situ chemical oxidative polymerization [10]. The high specific capacitance of 482 F g^{-1} was obtained from galvanostatic charge/discharge at a current density of 0.5 A g^{-1}. However, the power density of the composite only reached the range of 55–5510 W kg^{-1}. The less power density can result from less electronic conductivity of PPy prepared by chemical oxidative polymerization. At present, it is still very difficult for researchers to prepare the conducting polymer/graphene composite with high specific energy and specific power simultaneously.

In previous works, our group prepared the pure PPy by pulse current, showing high specific power, high specific energy and very good stability in 3 M HCl [6]. However, the capacitance on unit area electrode increased very small when the polymerization charge increased, which can result from the compact structure of pure PPy. In this work, RGO–PPy composite was prepared by in situ galvanostatic polymerization for supercapacitors electrode. Fig. 1 shows schematic diagram for the polymerization of

* Corresponding author. Tel.: +86 029 82665161; fax: +86 029 82665161.
E-mail address: ylxuxjtu@mail.xjtu.edu.cn (Y. Xu).

0378-7753/$ – see front matter © 2012 Elsevier B.V. All rights reserved.
doi:10.1016/j.jpowsour.2012.02.018

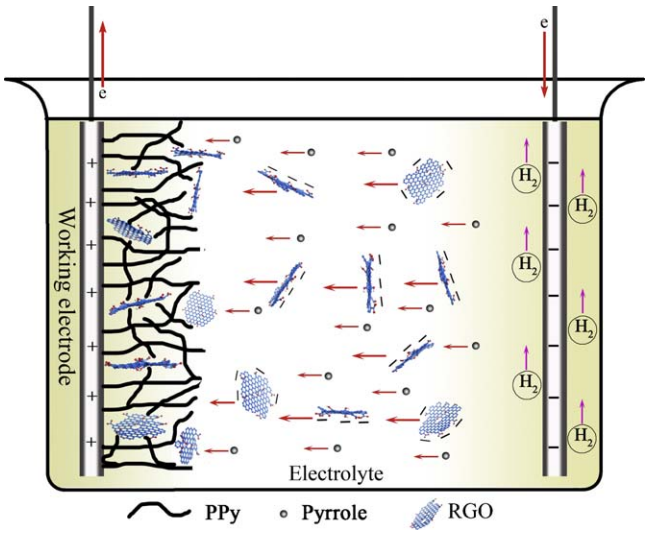

Fig. 1. Schematic diagram for the polymerization of RGO–PPy.

RGO–PPy. The RGO sheet moved toward the anode surface due to the negative charge on RGO sheet in aqueous solution (pH > 3) [15]. During PPy polymerization, the RGO sheets were embedded into PPy matrix, which formed the RGO–PPy composite with porous structure. The RGO–PPy composite was characterized by Raman spectroscopy, transmission electron microscopy (TEM), field emission scanning electron microscope (SEM) and X-ray photoelectron spectroscopy (XPS). The electrochemical performance of composite was investigated by cyclic voltammetry (CV), galvanostatic charge/discharge (GCD) and electrochemical impedance spectroscopy (EIS). The results indicated that the RGO–PPy electrode showed high specific power of 38.6 kW kg^{-1} when its specific energy reaches 2.5 Wh kg^{-1} in two-electrode cell. Furthermore, the capacitance on unit area RGO–PPy electrode increased obviously with the polymerization charge increasing.

2. Experimental

2.1. Reagents and materials

Pyrrole (Capchem, 99.8%) was distilled prior to use and stored at −10 °C in a nitrogen atmosphere. All other chemicals were reagent grade and used as received.

2.2. Preparation of composite

The RGO–PPy composites were prepared by in situ electrochemical polymerization. Graphite oxide was prepared by modified Hummers method from expanded graphite according to the literature [14]. RGO was prepared by reduction of graphene oxide with hydrazine hydrate according to the literature [15] and the concentration of RGO was 2 g L^{-1}. Sodium p-toluenesulfonate (PTSS, 2.33 g) was added to 40 mL deionized water and stirred for 10 min. The pH value of solution was adjusted to 3–7 by addition the p-toluenesulfonate acid (PTSA). The freshly distilled pyrrole (0.3 mL) was added into the solution and stirred rapidly for 5 min. Finally, the RGO aqueous suspension (2 mL) was added to the solution and sonicated for 15 min. Polymerizations was performed by a direct current in a three-electrode electrochemical cell, including a working electrode of 1 cm × 1 cm polished tantalum sheet, a reference electrode of standard calomel electrode (SCE) and a counter electrode of platinum sheet. All polymerizations were performed at a current density of 2 mA cm^{-2} for 500 s, 1000 s and 1500 s in an ice-water bath. The polymerization charge was 1 C cm^{-2}, 2 C cm^{-2} and 3 C cm^{-2}, respectively. The polymerization charge of samples in Raman spectroscopy, TEM, SEM, XPS, BET, CV, GCD, EIS and discharge capacitance retention measures were all 1 C cm^{-2}. The PPy mass was calculated by reference [5].

2.3. Characterization and electrochemical measurements

Raman spectroscopy was recorded using a micro-Raman LabRAM HR800 spectrometer (HORIBA Jobin Yvon) with X50WL objective and excited by 514 nm laser light. The incident laser was focused to a 2 μm spot and power of the laser was 2 mW. X-ray photoelectron spectroscopic measurements were performed with an AXIS-ULTRA DLD (Al Ka X-ray source, 1486.60 eV). All binding energies were referenced to the C 1 s neutral carbon peak set at 284.6 eV to compensate for surface charging effects. The structure of composite and PPy was investigated using transmission electron microscopy (JEOL, JEM-2100) with an accelerating voltage of 200 kV. The morphology of PPy films was investigated by field emission scanning electron microscope (JEOL, JSM-6700F) with an accelerating voltage of 5 kV. The surface area of RGO–PPy and PPy was determined using a BECKMAN COULTERAUT SA3100. The samples were dried at 100 °C for 5 h before measurement and degassed at 130 °C for 6 h until the vacuum was less than 10^{-3} Torr.

The electrochemical performance of composite was investigated by CV, GCD and EIS techniques, which were carried out in three-electrode system including a 1 cm × 1 cm working electrode, a counter electrode of platinum sheet and a reference electrode of SCE. The symmetrical two-electrode cells were assembled with for long term cycle stability test of PPy and composite, and the distance between two electrodes was 1 mm. All electrochemical tests were performed on the Versatile Multichannel Potentiostat 2/Z (VMP2, Princeton applied research) in 3 M KCL. EIS measurements were performed at 0 V (versus SCE) in the frequency range from 10^5 Hz down to 10^{-2} Hz, using an ac amplitude of 10 mV.

3. Results and discussion

The morphology, structure and electrochemical performance of RGO–PPy composite were closely related to the pH value of electrolyte, the concentration of RGO and the current density of polymerization. In our previous works, we found the low pH value (<1) and the high concentration of RGO (0.2 g L^{-1}) in polymerization electrolyte will result in the quick agglomeration of RGO. The electrochemical performance of RGO–PPy will decay when the high pH value of polymerization electrolyte was more than 9. It was difficult for RGO to deposit on Ta electrode when the current density of polymerization was less than 1 mA cm^{-2}. The porosity of RGO–PPy composite decreased when the current density of polymerization was more than 8 mA cm^2. Therefore, the pH value of electrolyte, the concentration of RGO and the current density of polymerization in this work were determined as 3–7, 0.1 g L^{-1} and 2 mA cm^{-2}, respectively.

Raman spectra are often used to characterize graphene samples. Fig. 2 shows Raman spectra of RGO, GO, PPy and RGO–PPy composite. The Raman spectra of RGO, GO include the high intensity of G band at 1583 cm^{-1} and D band at 1353 cm^{-1}, caused by the in-plane optical vibration and first-order zone boundary phonons, respectively [13]. Furthermore, a 2D band at 2690 cm^{-1} is observed in the Raman spectra of RGO, which corresponds to second-order zone boundary phonons [13]. The Raman spectra of PPy include the peaks at 977 cm^{-1}, 1050 cm^{-1}, 1350 cm^{-1} and 1578 cm^{-1}. The small peaks near 977 cm^{-1}, 1050 cm^{-1} have been associated with the polaron structure [18,19]. The broad peaks near 1350 cm^{-1} and 1578 cm^{-1} should correspond to ring stretching mode of the polymer backbone and π conjugated structure, respectively [18,19].

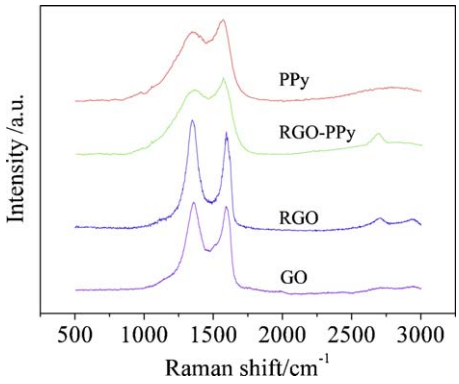

Fig. 2. Raman spectra of PPy and RGO–PPy composite.

However, in the Raman spectra of RGO–PPy composite, the new peak can be indexed at 2686 cm^{-1}, which should be 2D peak of RGO in composite [13,16]. The broad 2D band in the Raman spectra of RGO–PPy indicates that RGO in composite may be a multilayer structure [13].

TEM and SEM were used to study the morphology and structure of RGO, PPy and RGO–PPy composite. Fig. 3 shows TEM images of RGO, PPy and RGO–PPy composites. TEM image (Fig. 3a) shows typical single-layer and multi-layer RGO structure. The electron diffraction pattern in Fig. 3a has a well-defined sixfold-symmetry, which is similar to that of peeled-off graphene [20]. Fig. 3b shows the TEM image of PPy. The electron diffraction pattern in Fig. 3b indicates the PPy is amorphous structure. Fig. 3c shows the TEM image of RGO–PPy composite. The RGO–PPy composite has pronounced edges, which may be attributed to the embedment of single-layer and multi-layer RGO in composite matrix. The electron diffraction pattern in Fig. 3c confirms that the composite contains the components with crystal structure, such as single-layer and multi-layer RGO. Fig. 3d shows the TEM image of RGO–PPy edge with the bigger magnification. Noting that the edge of RGO–PPy composite includes ordered structure, which may be the embedded RGO in composite matrix. The electron diffraction pattern in Fig. 3c and d is similar to that of graphene/graphite with a typical sixfold symmetry characteristic [21], which confirms that the component with ordered structure in composite may be RGO.

Fig. 4 shows SEM images of PPy and RGO–PPy composite. The surface of PPy exhibits the typical 'cauliflower' structures in Fig. 4a, whereas the surface of RGO–PPy composite exhibits porous structure in Fig. 4b. In addition, the RGO seem to be closely surrounded by PPy, which can results from the intense interaction between PPy and RGO, such as π–π stacking, hydrogen bonding, van der Waals force and physical forces [9]. A lot of pores on electrode surface can enhance the capacitance and charge/discharge rate of RGO–PPy electrode. The nitrogen adsorption and desorption of RGO–PPy and PPy exhibit type IV characteristics in Fig. 5. Noting that the Brunaure–Emmett–Teller (BET) specific surface area of RGO–PPy (108 $m^2\ g^{-1}$) is much bigger than that of pure PPy (2.6 $m^2\ g^{-1}$). Therefore, more active material on RGO–PPy electrode can contacts with the electrolyte, which should enhance the specific capacitance of RGO–PPy. In addition, it is certain that the counterions obtain more channels of entering the PPy matrix, which can improve the charge/discharge rate of RGO–PPy electrode.

Fig. 6 presents the nitrogen 1s (N 1s) XPS core level spectrum of PPy and RGO–PPy composite. These core level spectrums show relatively broad peaks, indicating the existence of several

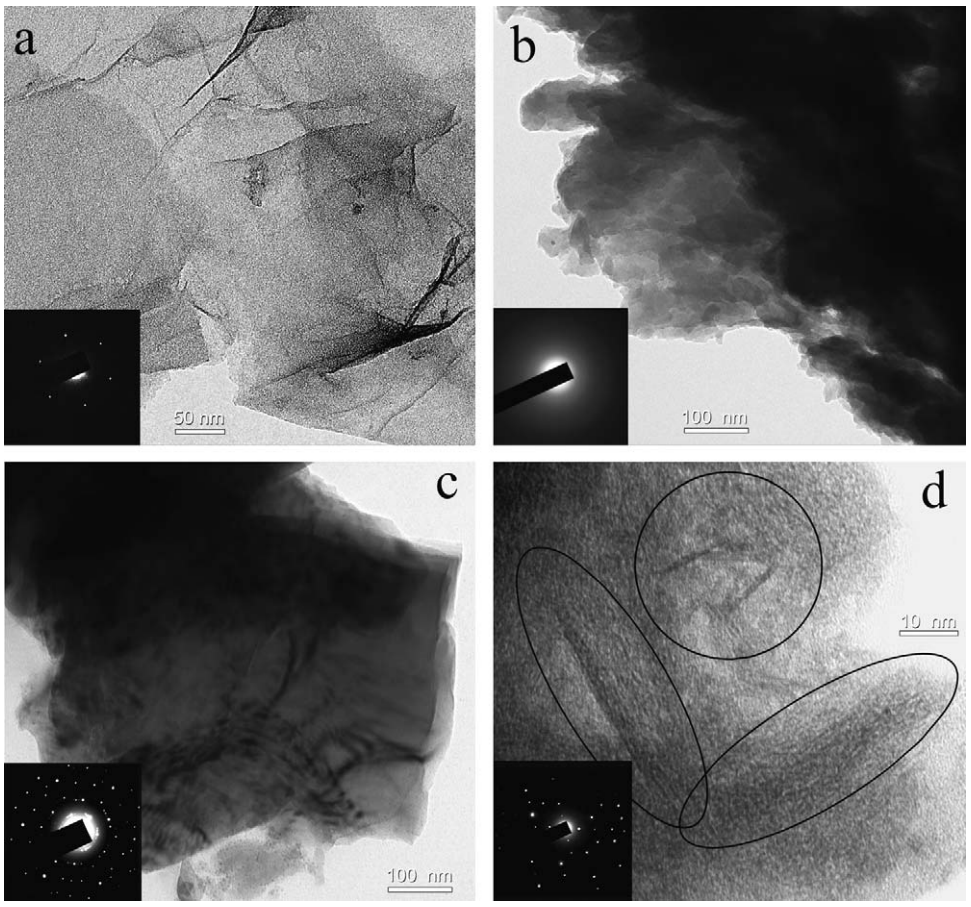

Fig. 3. TEM images of (a) RGO, (b) PPy, (c) and (d) RGO–PPy composite.

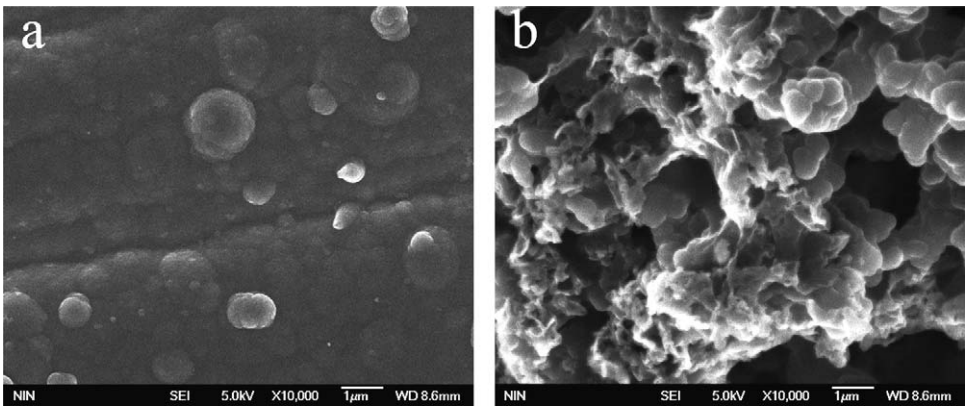

Fig. 4. SEM images of (a) PPy and (b) RGO–PPy composite.

structures. The decomposed peaks of N 1s at 399.95 ± 0.1, 401.1 ± 0.1 and 402.4 ± 0.2 should be attributed to benzenoid amine (–NH–), protonation benzenoid amine (–NH^+–) and protonation quinonoid imine (=NH^+–) [10,20]. The quinonoid imine structure is used to estimate the density of defect in PPy matrix [22]. The two spectrums do not show the peak at 398.3 ± 0.1 caused by quinonoid imine (=N–). This indicated the PPy prepared at low temperatures has few defects [23]. The shoulder on the higher energy side is considered as an electrostatic effect of the nearest counterions [22]. The electrostatic effect of PPy is relatively weak compared to that of RGO–PPy composite. The protonation level on the nitrogen site is 35.3% and 41.1% for PPy and RGO–PPy composite, respectively. Except the many doped ion of p-toluenesulfonate anion in PPy matrix, the PPy in composite can be doped by the oxygen-containing groups bonded in RGO sheet. This may be responsible for the higher protonation level on the nitrogen site in composite. The higher protonation level can improve the electrical conductivity of RGO–PPy electrode.

The CV curves were widely used to describe the electrochemical characteristic of electrode for supercapacitors [5,10]. Fig. 7 shows CV curves of PPy and RGO–PPy electrode in a three-electrode system. In Fig. 7a, the CV curve of RGO–PPy electrode shows rectangular shape, characteristic for an ideal capacitor at a high scan rate of $100\,mV\,s^{-1}$. This indicates a high rate of electrochemical process occurred in RGO–PPy electrode. Even at a very high scan rate of $1000\,mV\,s^{-1}$, the CV curve of RGO–PPy electrode shows about rectangular shape in Fig. 7b, whereas the CV curve of PPy shows cone shape. The high rate of electrochemical process means the quick diffusion of counterions and electrons in RGO–PPy matrix. Many pores on surface of RGO–PPy electrode should promote the diffusion of counterions.

Fig. 8 shows GCD curves of PPy and RGO–PPy electrodes in a three electrode system. In Fig. 8a, the specific capacitance of RGO–PPy electrode is more than two times of PPy specific capacitance at charge/discharge current density of $30\,A\,g^{-1}$. In Fig. 8c, with the increase of GCD current density, the specific capacitance decay of RGO–PPy electrode is obviously slower than that of PPy electrode. As the charge/discharge current density increasing from $30\,A\,g^{-1}$ up to $240\,A\,g^{-1}$, the decline of specific capacitance for RGO–PPy electrodes is only 15%, but the decline for PPy electrode approaches 47%. The specific capacitance RGO–PPy electrode still reaches $224\,F\,g^{-1}$ at charge/discharge current density of $240\,A\,g^{-1}$, whereas the specific capacitance PPy electrode only reaches $74\,F\,g^{-1}$, which is less than one third of RGO–PPy specific capacitance. The high specific capacitance of RGO–PPy electrode should be attributed to a lot of pores on electrode surface. The IR drop of RGO–PPy electrode in Fig. 8b is about one third of PPy IR drop at charge/discharge current density of $240\,A\,g^{-1}$. The less IR drop of RGO–PPy electrode must be associated with the good transport of electron and counterions in RGO–PPy matrix.

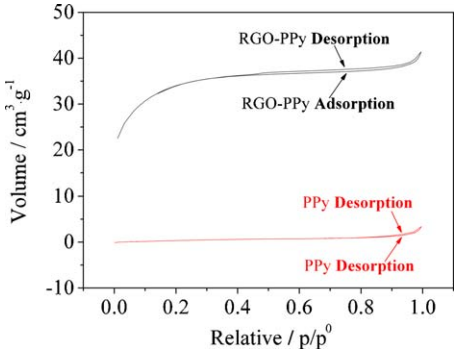

Fig. 5. Nitrogen adsorption and desorption isotherms.

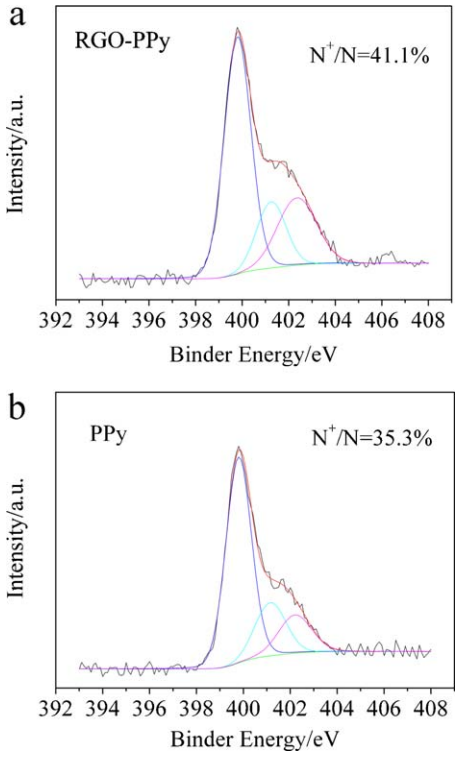

Fig. 6. Nitrogen 1s (N 1s) XPS core level spectrum of (a) RGO–PPy composite and (b) PPy.

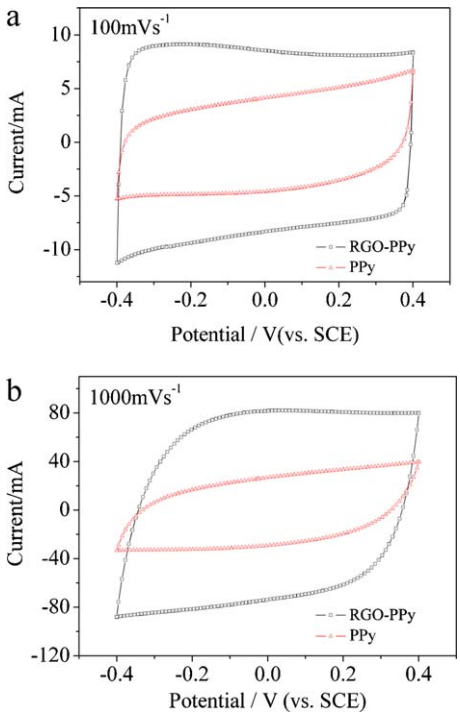

Fig. 7. CV curves of the PPy and RGO–PPy electrode in three electrodes cell at various scanning rates: (a) 100 mV s^{-1} and (b) 1000 mV s^{-1}.

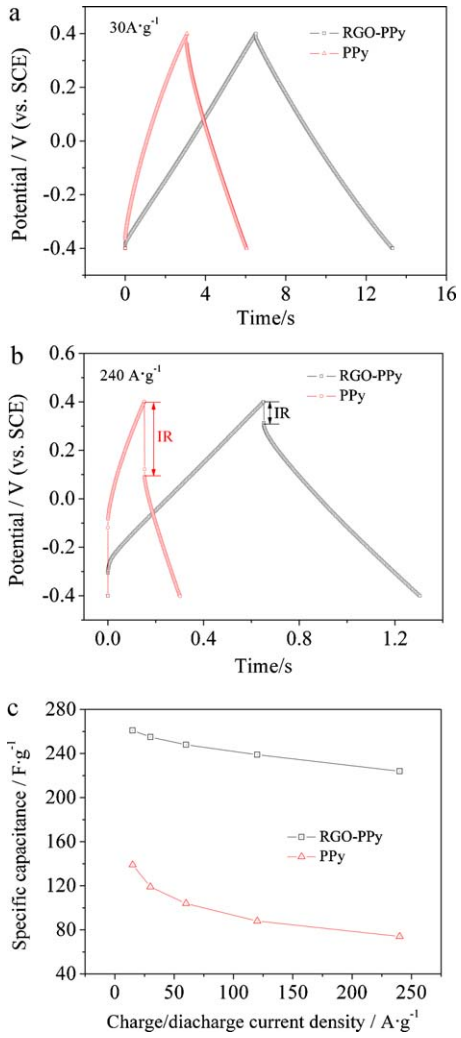

Fig. 8. GCD curves of PPy and RGO–PPy electrodes at different current density of (a) 30 A g^{-1}, (b) 240 A g^{-1} in three electrodes cell, (c) the specific capacitance of the PPy and RGO–PPy electrodes at different GCD current density.

Fig. 9 shows the specific capacitance change of PPy and RGO–PPy electrodes with the increase of the polymerization charge of active material. The specific capacitance of PPy and RGO–PPy electrodes was calculated when the CV scan rate was 100 mV s^{-1} with a 0.8 V electrochemical window. When the polymerization charge increase from 1 C cm^{-2} to 3 C cm^{-2}, the specific capacitance of PPy decreased 62%, whereas the specific capacitance of RGO–PPy only decreased 31%. The compact structure of PPy prepared by direct current effectively restricts counterions diffusion into PPy internal matrix, which results in the small increase of PPy capacitance on 1 cm^2 electrode and rapid decrease of PPy specific capacitance when the active material increases. The porous structure of RGO–PPy should promote counterions diffusion into PPy internal matrix, so the decrease of RGO–PPy specific capacitance is obviously smaller than that of PPy specific capacitance when the active material increases.

EIS is widely used to investigate the redox (charge/discharge) processes of electrode materials and to evaluate their electronic and ionic conductivities [6,9,10]. Fig. 10 shows the EIS curves of PPy and RGO–PPy electrodes in a three-electrode system. The EIS curves include a low-frequency region (straight line) and a high-frequency region (arc). The vertical shape at lower frequencies indicates an ideal capacitive behavior in electrode matrix [3]. The series resistance (R_s) includes both the solution resistance and the DC resistance [10]. The R_s of RGO–PPy electrode (0.21 Ω) is far less than that of PPy (1.37 Ω), which indicates RGO–PPy have better electronic transport ability. The high frequencies region is magnified and embedded into the blank. The diameter of arc at high frequencies is the charge transfer resistance (R_{ct}), which relates to interfacial processes of counterions through the electrode/electrolyte interface [7]. The R_{ct} of RGO–PPy electrode was only 0.26 Ω and is obviously less than that of PPy (0.5 Ω), meaning counterions with a higher rate pass the electrode/electrolyte interface into RGO–PPy matrix. The porous electrode with nanostructure usually shows the behavior of a planar electrode [24,25]. The very small R_{ct} of RGO–PPy electrode should be attributable to the highly porous structure of RGO composite. Therefore, EIS results indicated the RGO–PPy composite have good ionic and electronic transport ability.

Fig. 11 shows the simplified ragone plot of RGO–PPy and PPy calculated from galvanostatic discharge curves in two-electrode system. At same specific power density, the RGO–PPy electrode exhibits much higher specific energy than that of PPy electrode. The specific power of RGO–PPy is in the range of 1.5–38.6 kW kg^{-1}, when its specific energy is in the range of 2.5–5.7 Wh kg^{-1}. The

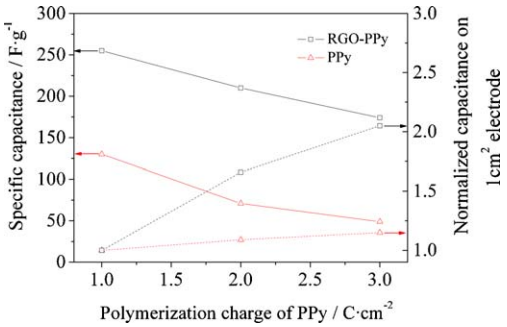

Fig. 9. The specific capacitance of PPy with different polymerization charge (the specific capacitance was calculated when the CV scan rate was 100 mV s^{-1}).

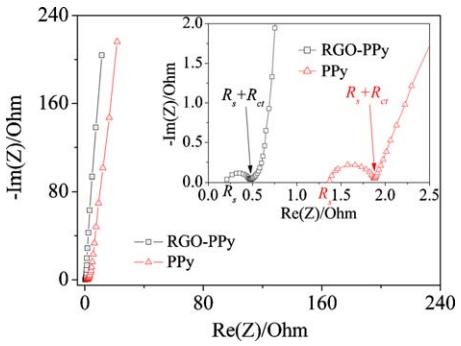

Fig. 10. EIS curves of the PPy and RGO–PPy electrode in three-electrode cell.

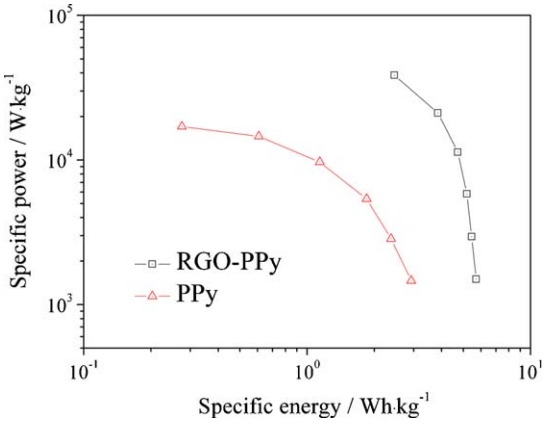

Fig. 11. Ragone plot of RGO–PPy and PPy.

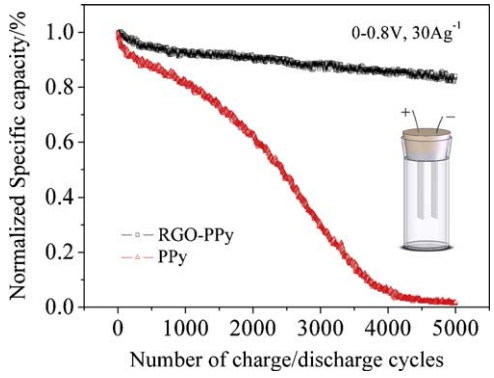

Fig. 12. Discharge capacitance retention for the PPy and RGO–PPy electrode at a charge/discharge current of 30 A g^{-1} within a voltage range of 0–0.8 V.

specific power of RGO–PPy shows a maximum value of 38.6 kW kg^{-1} when its specific energy reaches 2.5 Wh kg^{-1}.

At present, the discharge capacitance retention is the key to the commercialization of PPy supercapacitors. Fig. 12 shows discharge capacitance retention for PPy and RGO–PPy electrodes at a charge/discharge current of 30 A g^{-1} within a voltage range of 0–0.8 V in a symmetrical two-electrode cell. The model capacitor for cyclic stability test is shown in Fig. 12. Compared with the PPy electrode, the RGO–PPy electrode is stable in 3 M KCl, showing less than 17% decay after 5000 cycles. While the PPy capacitance rapidly decreases to 3–5% after 5000 cycles. RGO has high Young's modulus and good stable [13], so the embedded RGO in composite, on one hand, improves mechanical properties of composite, and on the other hand, reduces the change of volume in oxidation/reduction process. Therefore, the RGO–PPy composite prepared by in situ electrochemical polymerization can be a very potential material for the electrode of supercapacitors.

4. Conclusion

The RGO–PPy composites were prepared by in situ electrochemical polymerization for supercapacitors electrode. The RGO–PPy electrodes exhibited high specific capacitance, good rate performance and cyclic stability. The embedment of RGO in composite resulted in the porous structure on composite surface and the high protonation level on PPy ring, which may be the main reason of good ionic and electronic transport ability in composite matrix. The high specific capacitance of RGO–PPy electrode was closely related to the porous structure and the high protonation level on PPy ring in composite matrix. The embedment of RGO improved the cyclic stability of PPy electrode, showing less decay at a charge/discharge current of 30 A g^{-1} after 5000 cycles. The RGO–PPy composite should be a very potential material for the electrode of supercapacitors.

Acknowledgements

The authors wish to thank for the financial supports by the National High Technology Research and Development Program of China (Grant No. 2007AA03Z249), the National Natural Science Foundation of China (Grant No. 20804030 and No. 51073128), the Shaanxi National Science Foundation (Grant No. 2011JM6003).

Appendix A. Supplementary data

Supplementary data associated with this article can be found, in the online version, at doi:10.1016/j.jpowsour.2012.02.018.

References

[1] D. Pech, M. Brunet, H. Durou, P. Huang, V. Mochalin, Y. Gogotsi, P.-L. Taberna, P. Simon, Nat. Nano 5 (2010) 651.
[2] C. Liu, Z. Yu, D. Neff, A. Zhamu, B.Z. Jang, Nano Lett. 10 (2008) 4863.
[3] M.D. Stoller, S. Park, Y. Zhu, J. An, R.S. Ruoff, Nano Lett. 8 (2008) 3498.
[4] P. Simon, Y. Gogotsi, Nat. Mater. 115 (2008) 845.
[5] C.C. Hu, X.X. Lin, J. Electrochem. Soc. 149 (2002) A1057.
[6] J. Wang, Y. Xu, J. Wang, X. Du, Synth. Met. 161 (2011) 1141.
[7] C. Debiemme-Chouvy, T.T.M. Tran, Electrochem. Commun. 10 (2008) 947.
[8] A. Izadi-Najafabadi, D.T.H. Tan, J.D. Madden, Synth. Met. 152 (2005) 129.
[9] K. Jurewicz, S. Delpeux, V. Bertagna, F. Beuin, E. Frackowiak, Chem. Phys. Lett. 347 (2001) 36.
[10] D. Zhang, X. Zhang, Y. Chen, P. Yu, C. Wang, Y. Ma, J. Power Sources 196 (2011) 5990.
[11] S. Biswas, L.T. Drzal, Chem. Mater. 22 (2010) 5667.
[12] J.Y. Kim, K.H. Kim, K.B. Kim, J. Power Sources 176 (2011) 396.
[13] Y. Zhu, S. Murali, W. Cai, X. Li, J.W. Suk, J.R. Potts, R.S. Ruoff, Adv. Mater. 22 (2010) 3906.
[14] P. Ren, D. Yan, X. Ji, T. Chen, Z. Li, Nanotechnology 22 (2011) 055705.
[15] D. Li, M.B. Muller, S. Gilje, R.B. Kaner, G.G. Wallace, Nat. Nano 3 (2008) 101.
[16] C.N.R. Rao, A.K. Sood, K.S. Subrahmanyam, A. Govindaraj, Angew. Chem. Int. Ed. 48 (2009) 7752.
[17] Q. Cheng, J. Tang, J. Ma, H. Zhang, N. Shinya, L. Qin, Carbon 49 (2011) 2917.
[18] J. Mikat, I. Orgzall, H.D. Hochheimer, Phys. Rev. B 65 (2002) 174202.
[19] S. Demoustier-Champagne, P.Y. Stavaux, Chem. Mater. 11 (1999) 829.
[20] W. Zhang, J. Cui, C. Tao, Y. Wu, Z. Li, L. Ma, Y. Wen, G. Li, Angew. Chem. 121 (2009) 5978.
[21] Y. Wang, Z. Shi, J. Fang, H. Xu, X. Ma, J. Yin, J. Mater. Chem. 21 (2011) 505.
[22] J. Joo, J.K. Lee, S.Y. Lee, K.S. Jang, E.J. Oh, A.J. Epstein, Macromolecules 33 (2000) 5131.
[23] M. Osagawara, K. Funahashi, T. Demura, T. Hagiwara, K. Iwata, Synth. Met. 14 (1986) 61.
[24] W. Sugimoto, H. Iwata, K. Yokoshima, Y. Murakami, Y. Takasu, J. Phys. Chem. B 109 (2005) 7330.
[25] C.C. Hu, H.Y. Guo, K.H. Chang, C.C. Huang, Electrochem. Commun. 11 (2009) 1631.